

Density Functional Theory Study of the Entangled Crystal, Magnetic, and Electronic Structures of PuGa_3

Sven P. Rudin

Los Alamos National Laboratory, Los Alamos, New Mexico 87545, USA

(Dated: February 25, 2022)

Abstract

Systematically studying the crystal, magnetic, and electronic structures of PuGa_3 with density functional theory (DFT) reveals the entanglement of the three types of structure. Magnetic structure affects the energy more strongly than crystal structure. For DFT to correctly order the crystal structures in agreement with experiment requires special treatment of the electronic correlation in the $5f$ states, exemplified here by the GGA+U approach. The upper and lower Hubbard bands change with increasing U in very dissimilar ways for the two most different crystal structures. The results suggest the effectiveness of using magnetic structure to simulate correlation effects in the actinides depends on both the magnetic and the crystal structure.

PACS numbers: 71.27.+a, 71.10.Fd

I. INTRODUCTION

PuGa_3 appears in two crystal structures with similar electronic structures but different magnetic structures. Ellinger *et al.* noted in 1964 the appearance of the two crystal structures and identified the low-temperature (low- T) form as hexagonal and isostructural with Ni_3Sn ;¹ the following year Larson *et al.* identified the high-temperature (high- T) form as a 12-layer rhombohedral close-packed structure with space group $R\bar{3}m$.² Four decades later, magnetic measurements revealed the low- T form to be an antiferromagnet ($T_N = 24$ K) and the high- T form to be a ferromagnet ($T_C = 20$ K), and specific heat measurements suggest for both phases an electronic structure with heavy fermion character.³

These characteristics place PuGa_3 in compelling relation to other heavy fermion systems of significant interest. The electronic specific heat coefficient γ , a measure of the electronic density of states at the Fermi energy, has values (220 and 100 mJ/mol K² for low- T and high- T , respectively) similar to the heavy fermion superconductors PuCoGa_5 and PuRhGa_5 .⁴ Neither of these are magnetic experimentally, though electronic structure calculations favor antiferromagnetic order.⁵ With rather delocalized $5f$ electrons, PuGa_3 lies between PuCoGa_5 and $\delta\text{-Pu}$,³ which has more localized $5f$ electrons but also shows no localized magnetic moments.⁶

The combination of magnetic structure and heavy fermion behavior in PuGa_3 suggest a challenging system for electronic structure calculations. The electronic structure of Pu, many Pu compounds, and some other actinide systems requires special attention to be paid to the strong $5f$ electron correlation. Calculations with “standard” density functional theory (DFT) methods, which involve limited approximate treatments of the electronic correlation, favor an antiferromagnetic structure,^{7–9} and some aspects are even better modeled with disordered local moments or approximations thereof.^{10,11} Experimentally, pure Pu shows no signs of magnetic moments.⁶ The breaking of spin symmetry in DFT calculations delivers a static approximation of the spatial separation experienced by dynamically correlated electrons. As a result, calculations allowing a localized magnetic moment can be used to explore nonmagnetic aspects of Pu and Pu compounds without introducing material-dependent parameters. The existence of magnetic structures in PuGa_3 entangles the magnetic moments and the electronic correlation, which, along with their entanglement with the observed crystal structures, motivates this study.

The crystal structures of PuGa_3 can be viewed as close-packed PuGa_3 planes with different stacking sequences.² The low- T structure follows an AB sequence, as does hexagonal close packed (hcp); stacking in the high- T structure progresses as ABABCACABCBC (with some in-plane distortions away from the perfect close-packed planar structures). This layered, close-packed nature already appears in crystal structures of pure Pu: the face-centered cubic structure of δ -Pu exhibits ABC stacking, the Crocker pseudostructure for α -Pu follows from the α structure's repeating two planes of a distorted hexagonal structure,¹² and the orthorhombic structure of γ -Pu exhibits close-packed Pu planes stacked such that Pu atoms in one plane sit above bonds in the plane underneath (giving rise to an ABCD stacking pattern). The close-packed PuGa_3 planes correspond to the close-packed Pu planes with ordered substitutional placing of Ga.

These stacking sequences of close-packed planes (excluding that of γ -Pu) can also be written as sequences of shifts between planes: AB, BC, CA being shifts to the right (R) and AC, CB, BA being shifts to the left (L). ABC stacking always shifts in the same direction (RRRR), AB stacking alternates between the two directions (RLRL), and ABABCACABCBC stacking, rewritten as (ABCA)(CABC)(BCAB), reverses direction once every four planes (RRRL). The missing unique pattern with four shifts, RRLL, is ABCB stacking, which corresponds to double hcp (dhcp), exemplified by α -La.

While the R and L shifts are equivalent, a stark difference exists between a plane that links two shifts with the same direction and one that sits at a reversal in the direction. The local environment of the atomic sites in the ideal close-packed lattices has twelve nearest neighbors in both cases. Sites in a plane between two identical shifts have the inversion symmetry, while those between two opposite shifts do not. The lack of inversion symmetry disrupts an otherwise straight line of bonding oriented 60° to the planes. A natural order of the four crystal structures arises: ABC stacking has no disruptions, AB stacking has disruptions in every plane, and the remaining two stacking sequences lie in between.

The work presented here applies DFT to reveal the interplay between crystal structures based on these four structural patterns, a series of magnetic structures, and the resulting electronic structures. Starting from “standard” DFT in the generalized gradient approximation (GGA), calculations furthermore explore the effects of adding either spin-orbit coupling or a Hubbard U (in the GGA+ U method). The calculations presented here set aside thermal effects, in particular those due to phonons. Preliminary calculations of the phonons

and their contribution to the free energy suggest they cannot make the low- T phase more favorable in the GGA to DFT without specifically addressing f electron correlation.

II. METHOD

The DFT calculations employ the VASP package.^{13,14} They make use of the generalized gradient approximation (GGA) of Perdew, Burke, and Ernzerhof.¹⁵ The Pu($5f, 6d, 7s$) and Ga($4s, 4p$) electrons are treated in the valence using a plane-wave basis and with projector-augmented wave potentials.¹⁶ The calculations employ Methfessel-Paxton smearing (with width 0.1 eV), a k-point mesh of density 40 \AA^{-1} , and an energy cutoff of 400 eV. The self-consistent cycles are converged to within 10^{-5} eV. Calculations aimed at improving the treatment of the on-site Coulomb repulsion between $5f$ electrons use an effective Hubbard parameter U in the rotationally invariant form of Dudarev *et al.*¹⁷ In this form the Hubbard parameter U and the exchange parameter J appear only in the difference $U - J$, throughout this report the difference is referred to as U . Calculations that include the effects of spin-orbit coupling do so in the noncollinear mode of VASP,^{18,19} the implementation follows the approach of Kleinman and MacDonald, Pickett, and Koelling.^{20,21}

The calculations optimize crystal structures that start as ideal close-packed planes with one Pu and three Ga atoms, stacked according to one of the four patterns described above. Relaxation of the structures retains the overall layered structure, but displacements within the planes make initially equivalent planes lose their exact equality. The size of the unit cell, in particular the number of planes (between two and twelve), follows from the particular pattern and the magnetic structure used to seed the calculations. The latter either has all spins in the same direction for the ferromagnetic (FM) structure, or spins that switch direction every one, two, three, four, or six planes. These arrangements define spin wave structures with wave vectors \mathbf{q} of magnitude $\frac{1}{1}, \frac{1}{2}, \frac{1}{3}, \frac{1}{4}, \frac{1}{6}$, and, in the FM case, $\frac{1}{\infty}$, scaled by $\frac{\pi}{c_0}$, where c_0 represents the interplanar spacing. Additional magnetic structure within the close-packed plane affects the results, but these are not reported here, other than to note that their energy lies above that of the antiferromagnetic (AFM, $|\mathbf{q}| = 1 \frac{\pi}{c_0}$) state.

III. RESULTS

The results from three approaches appear in the following three subsections. Sections III A and III B report the results of DFT calculations in the GGA without and with spin-orbit coupling, respectively, for the four crystal structures in a sequence of magnetic states. Section III C focuses on results of the GGA+U method applied to the low- T and cubic structures in the AFM state. Table I summarizes the energies, volumes and c/a ratios calculated in the three approaches for the four crystal structures in the AFM state.

A. DFT in the GGA

Figure 1 shows the interplay between the four crystal structures and the magnetic structures using the GGA to DFT. All four stacking sequence patterns show a preference for the magnetic structure with the shortest spin wave length, the AFM state. The ordering of energies of the crystal structures in the AFM state correlates with the order arising from the number of changes in R and L shifts mentioned in the introduction. With this magnetic structure, the experimentally observed low- T phase lies highest, 117 meV/PuGa₃ above the favored structure with ABC stacking. This cubic structure is observed for PuIn₃ and is often considered a building block for the layered superconductors PuCoGa₅, CePt₂In₇, Ce₂RhIn₈, etc. The preference for this cubic structure appears only for the magnetic structure with the shortest spin wave length; for longer spin wave lengths it lies higher than the other states (albeit by small amounts). Among the FM states the high- T phase lies lowest, the slight 13 meV/PuGa₃ difference to the low- T phase suggests the importance of thermal effects.

The optimized structures agree reasonably well with experimental volumes, while the optimized c/a ratios consistently lie above the experimental values. The AFM volume calculated for the low- T structure is only 1% smaller, but the c/a ratio is close to 6% larger than the experimental value (see Table I). The AFM volume calculated for the high- T structure is 0.25% smaller than the experimental value, and the c/a ratio is close to 4% larger than the experimental value. The FM volume calculated for the high- T structure is 1% larger, and the c/a ratio is 3% larger than the experimental value. The distances from Pu to nearest Ga atoms (located in adjacent planes) differ by negligible amounts between the calculated and experimental high- T structures. The larger calculated c/a ratio does

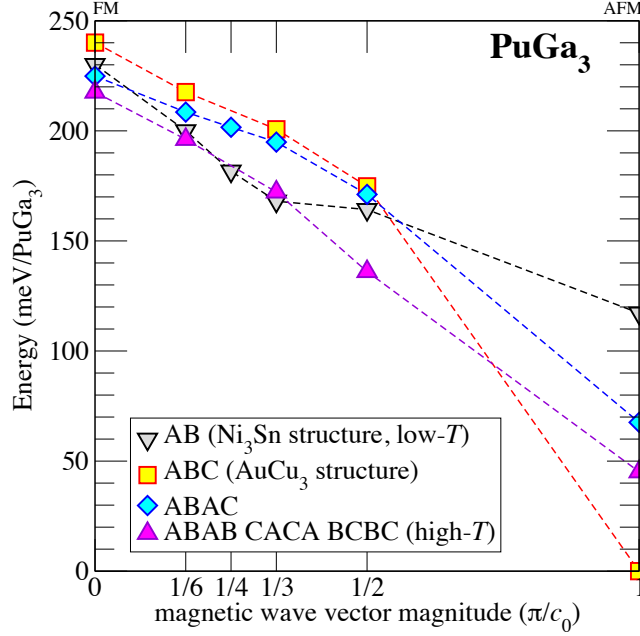


FIG. 1. (Color online) Calculated dependence of energy on stacking and magnetic structure for PuGa_3 using GGA ($U = 0$). Stacking denotes initial crystal structure; upon relaxation the planes with the same letter are no longer necessarily equivalent. Stacking direction corresponds to body diagonal of the conventional AuCu_3 crystal structure unit cell; the lowest energy appears for G-type antiferromagnetism (AFM(G)). Dashed lines serve to guide the eye.

affect the angle spanned by a Pu atom and two Ga atoms in adjacent planes, decreasing it by as much as 13%.

Figure 2(a) compares calculated total electronic densities of states (DOS) and suggests why the cubic structure appears more favorable in the AFM state. The low- T , high- T , and cubic structure differ significantly in the highest occupied states. The low- T and cubic structure both exhibit a single peak, but the cubic structure has it almost 0.3 eV further below the Fermi level E_F . The high- T structure exhibits a double peak centered between the other two structures. While the band energy is only one part of the total energy, this ability of the structures to push states down and away from E_F corresponds to their order in total energy.

Figure 2(b) plots the analogous comparison for the three structures in the FM state. Compared to the AFM state, the peaks appear much more similar for the three structures than in the AFM state. Accordingly, the total energies for the FM state differ by smaller

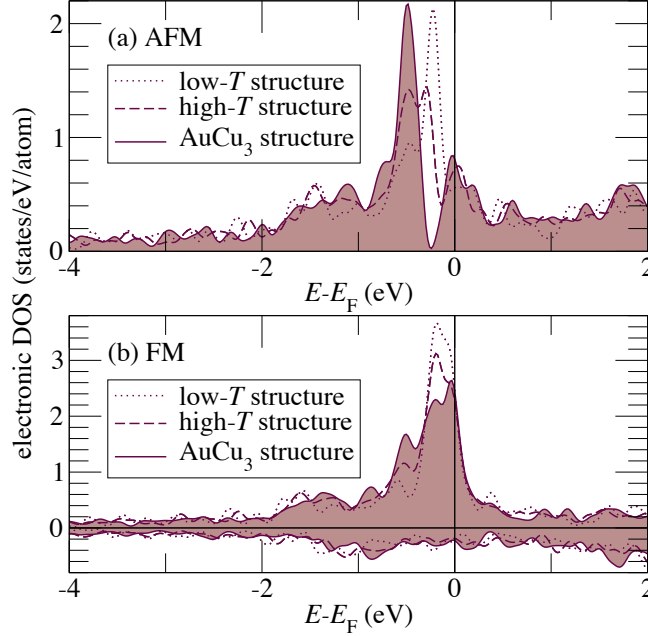


FIG. 2. (Color online) Calculated electronic densities of states (DOS) near the Fermi energy E_F using the GGA to DFT ($U = 0$) for low- T , high- T , and AuCu₃ crystal structures with (a) AFM and (b) FM structure. Only the DOS for one spin orientation appears for AFM.

amounts compared to the AFM state. The peaks sit closer to E_F in the FM state, concurring with the energies of the FM state lying higher than those of the AFM state.

Figure 3 shows the f symmetry character (projected out on a Pu site) of the electronic DOS calculated for the low- T and AuCu₃ crystal structures with AFM magnetic structure. The f -projected peaks correspond to the peaks in Fig. 2(a). The projected DOS are identical for all sites in each case, as expected given the sites' identical environments: each site has the same structural environment and nearest neighbors with opposite spin. The structural environment differs between the two cases, the AuCu₃ crystal structure's inversion symmetry allows the f -projected peaks to be pushed down lower. The less symmetric local environment in the low- T structure makes it less atomic-like, requiring the f electrons to hybridize more.

Figure 4 compares the f symmetry character projected out on Pu sites from the electronic DOS calculated for the low- T and AuCu₃ crystal structures in the magnetic state with spin wave vector magnitude $\frac{1}{6} \frac{\pi}{c_0}$. This choice of spin wave vector stems from the differences it reveals among the Pu sites, unlike the ferromagnetic structure where all sites (within each crystal structure) remain equivalent. For the low- T structure the projected electronic

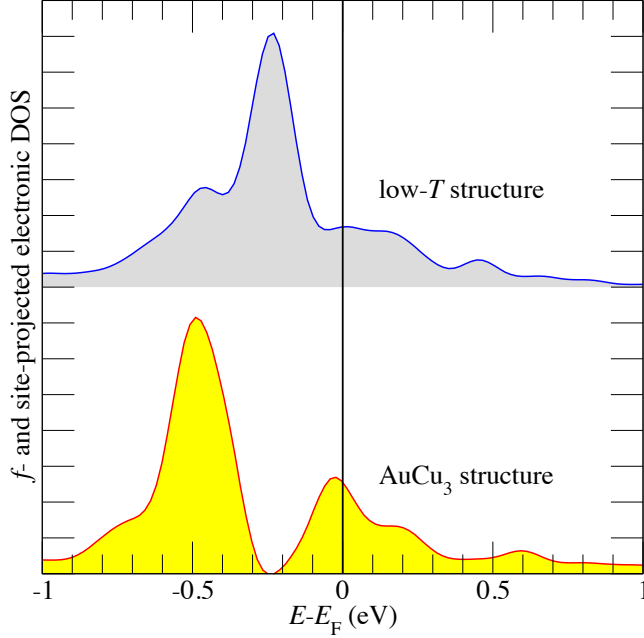


FIG. 3. (Color online) Calculated electronic DOS near E_F projected on a Pu site with f character using the GGA to DFT ($U = 0$) for low- T and AuCu₃ crystal structures with AFM magnetic structure. The plotted DOS represent the majority spin on the Pu site.

DOS differs only slightly between the three types of sites, a slight shift down from E_F occurs closer to the edge of the magnetic subdivision. The cubic structure shows dramatic differences between the three types of sites: all show a projected electronic DOS hugging E_F from below, and only the site at the edge of the magnetic subdivision appears able to spread a significant amount down several tenths of an eV. In the FM state, the f -projected DOS on any of the sites closely resembles the f -projected DOS shown here for center atoms.

B. including spin-orbit coupling

Figure 5 shows the interplay between the four crystal structures and magnetic structures using the GGA to DFT and including spin-orbit coupling. The inclusion of spin-orbit coupling reduces the energy differences overall, hence Figure 5 appears much like a scaled version of Fig. 1. The AuCu₃ crystal structure in the AFM state remains the most favored, in the FM state it remains the least favored.

Results from calculations that include spin-orbit coupling repeat the correlation between which structure is energetically favored and its ability to push electronic states down and

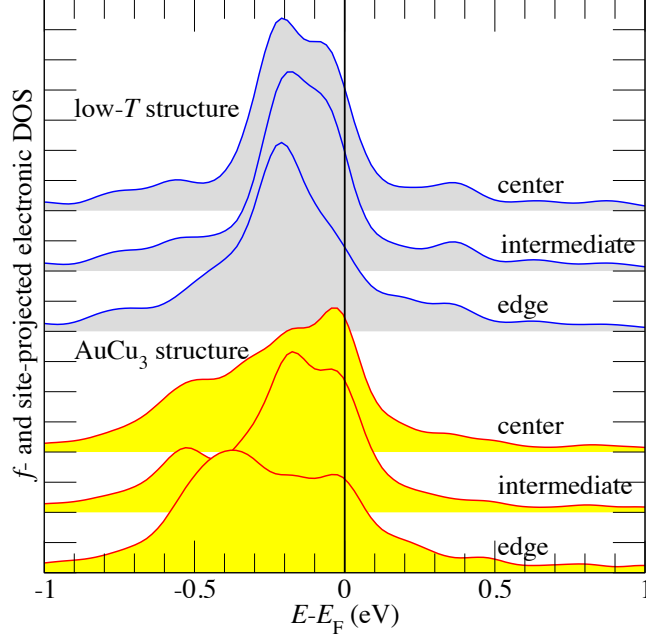


FIG. 4. (Color online) Calculated electronic DOS near E_F projected on Pu sites with f character using GGA ($U = 0$) for low- T and AuCu_3 crystal structures with magnetic structure that has spin wave length spanning twelve planes. The plotted DOS represent the majority spin on each site. In terms of geometry, all sites are equivalent for each crystal structure. They differ depending on where they sit within the magnetic structure: adjacent to the spin flip (“edge”), one layer farther in (“intermediate”), or most distant to the spin flip (“center”).

away from E_F . With spin-orbit coupling, the electronic DOS of the low- T and AuCu_3 crystal structure differ from one another less than in Fig. 2, but the more favored AuCu_3 crystal structure still succeeds better at pushing electronic states to lower energies.

C. including a Hubbard U

Table I shows how treating the on-site Coulomb repulsion between $5f$ electrons with a Hubbard U changes the ranking of crystal structures. Setting $U = 3$ eV reverses the sequence in energy from the GGA result (with or without spin-orbit coupling): the low- T crystal structure becomes most favored while the AuCu_3 crystal structure becomes the least favored. The high- T and “ α -La” structures remain in between and switch their order as well. Comparison of the energies for the different crystal structures only has meaning for each value of U individually, which is somewhat unsatisfactory since the different crystal structures

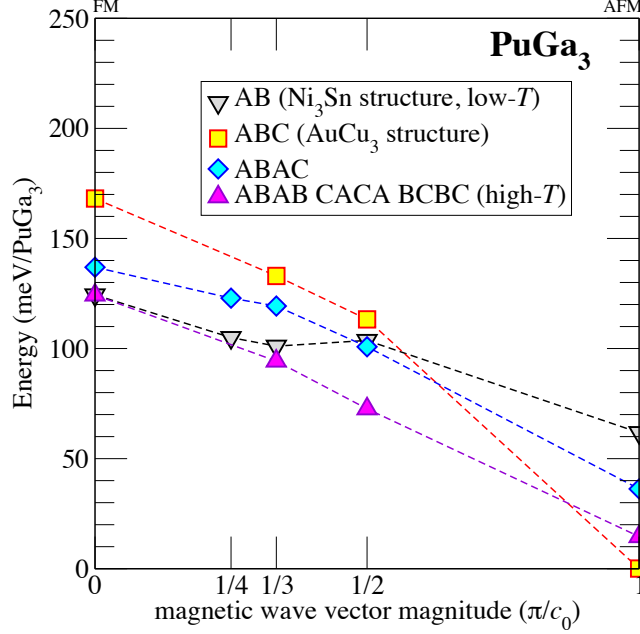


FIG. 5. (Color online) Calculated dependence of energy on stacking and magnetic structure for PuGa_3 using GGA ($U = 0$) and including spin-orbit coupling. Dashed lines serve to guide the eye. Notation follows Fig. 1.

would be better described with different values (differences in the electronic specific heat coefficient γ and in the Pu-Ga distances in the low- T and high- T crystal structure suggest different degrees of $5f$ delocalization,³ implying incompatible values of U).

Figure 6 plots the electronic DOS for the low- T crystal structure in the AFM state calculated with the GGA+ U method. As U increases, the dominant peaks, DFT's rendering of the upper and lower Hubbard bands,²² increasingly separate. This separation pushes the occupied states down from E_F more than it pushes the unoccupied states up. The symmetry between up and down spin remains intact, and, based on site-projected DOS (not shown here), the equivalence among sites with the same spin remains.

Figure 7 plots the electronic DOS for the AuCu_3 crystal structure in the AFM state calculated with the GGA+ U method. Again the increasing U drives the dominant peaks apart, but for this crystal structure the separation occurs mainly by pushing up the unoccupied states. The occupied states change little as U increases from 0 eV to 1 eV. Increasing U from 1 eV to 2 eV pushes the occupied states down. Setting $U = 3$ eV breaks the symmetries of up and down spins as well as the equivalence among sites with the same spin.

structure	U (eV)				SOC
	0	1	2	3	($U = 0$)
Relative energies (meV/PuGa ₃)					
low- T	0	0	0	0	0
“ α -La”	-49	-9	6	109	-26
high- T	-72	-53	-26	120	-47
AuCu ₃	-117	-67	2	168	-62
Volumes ($\text{\AA}^3/\text{PuGa}_3$)					
low- T	77.37	78.09	80.00	81.28	77.99
“ α -La”	77.59	78.58	79.78	80.84	77.52
high- T	77.50	78.22	79.68	80.90	77.50
AuCu ₃	77.72	77.72	79.88	80.77	77.67
c/a ratio					
low- T	0.38	0.38	0.37	0.36	0.37
“ α -La”	0.40	0.39	0.39	0.39	0.39
high- T	0.39	0.39	0.39	0.38	0.39
AuCu ₃	0.41	0.41	0.41	0.41	0.41

TABLE I. Relative energies, volumes, and c/a ratios for the structures calculated with DFT in the GGA with different values for U (without spin-orbit coupling) and for $U = 0$ eV with spin-orbit coupling (SOC). All results are for the AFM state. The measured values for the volume are 78.12 and 77.70 \AA^3 and for the c/a ratio are 0.358 and 0.378 for the low- T and high- T structures, respectively.³

Comparison of Figs. 6 and 7 for each value of U correlates well with the energy differences in Table I. For $U = 1$ eV the AuCu₃ crystal structure retains the peak around 0.5 eV below E_F while the low- T crystal structure has its main peak shifted lower than for $U = 0$. For $U = 2$ eV both crystal structures have shifted (and broadened) the peak to around 1 eV below E_F . For $U = 3$ eV the overall DOS changes somewhat for the AuCu₃ crystal structure while for the low- T crystal structure a dramatic shift downward occurs.

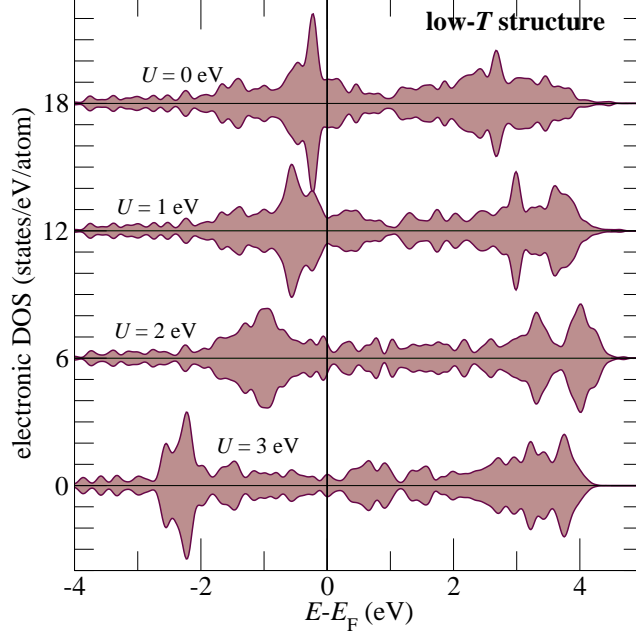


FIG. 6. (Color online) Calculated electronic DOS with varying Hubbard U for the low- T crystal structure with AFM magnetic structure at the experimental volume. The DOS for the two spin orientations appear as positive and negative, respectively.

IV. DISCUSSION AND CONCLUSIONS

Systematically studying the crystal and magnetic structures of PuGa_3 reveals how they affect the electronic structure and how the three types of structure are entangled. The key to understanding the entanglement lies in the position of the $5f$ electron states relative to the Fermi level E_F in the electronic DOS. The position relative to E_F is determined by both the symmetry of the crystal structure and the imposed magnetic structure. How far the $5f$ peak sits below E_F dovetails with how favorable the system in question is in terms of calculated total energy.

Magnetic structure affects the energy more strongly than crystal structure. With or without spin-orbit coupling, the calculations favor the AFM state over the FM state for all crystal structures. Spin density waves with wave lengths between those of the FM state

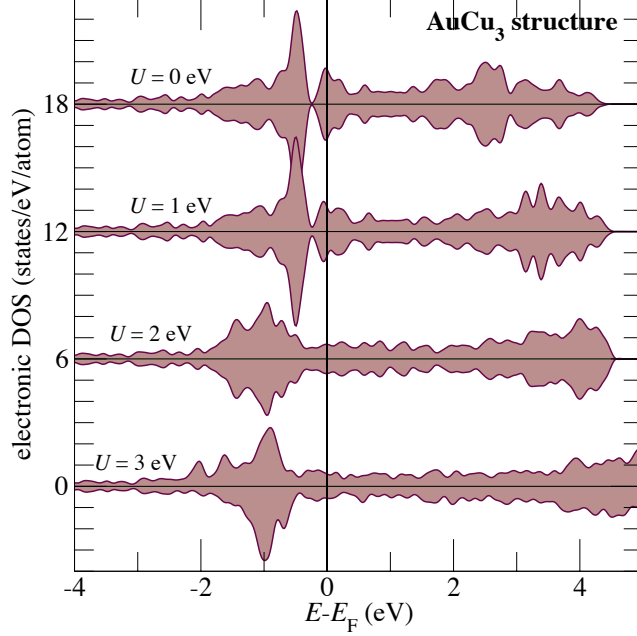


FIG. 7. (Color online) Calculated electronic DOS with varying Hubbard U for the cubic crystal structure with AFM magnetic structure at the experimental volume. The DOS for the two spin orientations appear as positive and negative, respectively. For $U=2$ eV and above the symmetry between Pu sites is broken and variations of up to 0.6% appear in the site-projected charge and of up to 5% appear in the site-projected magnetic moments.

(infinity) and of the AFM state (twice the spacing between Pu planes) give total energies between the two limiting values. Pu sites neighboring a junction between up and down spins have their $5f$ electron states farther below E_F than other Pu sites. Each such junction gives the sites sandwiching the junction less hybridization of $5f$ states with neighbors on the other side of the junction. In the limiting case of AFM, every site has the least hybridization because Pu sites in neighboring planes have opposite spin.

Calculations using standard GGA result in the wrong crystal structure (AuCu_3) having the lowest energy in the favored AFM state. The $5f$ electron states in the cubic structure sit farther below E_F than they do in the experimentally observed Ni_3Sn crystal structure, because the inversion symmetry at sites in the cubic structure requires less hybridization between the Pu $5f$ states and other states.

Adding a Hubbard U to treat the strong $5f$ electron correlation results in the correct crystal structure having the lowest energy. The U raises and lowers the potential acting on

the unoccupied and occupied $5f$ states, respectively, but the effect of U on the positions of the $5f$ states relative to E_F depends on how they are hybridized.²³ Increasing the value of U proves more effective at lowering the energy of the $5f$ electron peak for the Ni_3Sn crystal structure, making it most favored for $U = 3$ eV.

Allowing localized magnetic moments to simulate correlation effects fails for PuGa_3 . The strong preference for the cubic crystal structure over the hexagonal crystal structure suggests the failure stems not from the actual presence of a magnetic structure (observed in experiment), but from the symmetry at Pu sites in the hexagonal crystal structure being much lower than in the cubic crystal structure. The use of allowing localized magnetic moments to simulate correlation does so by permitting the $5f$ electrons on the same Pu site to occupy more orbitals that differ spatially. The inversion symmetry present in the cubic crystal structure makes the localized magnetic moments most effective at simulating correlation effects. In the hexagonal crystal structure the lower symmetry prevents an adequate decoupling of f states from hybridization and their energy cannot be lowered sufficiently to make the crystal structure most favorable.

These results suggest a explanation for the effectiveness of using magnetism to approximate correlation effects in δ -Pu. The crystal structure of δ -Pu is face-centered cubic, and all sites exhibit the inversion symmetry shown here to be important in the closely-related AuCu_3 structure. Given the similarities, the preference for an AFM state in δ -Pu does not surprise. Nor does the additional effectiveness of modeling correlation effects with disordered local moments astonish, since such a magnetic “structure” reduces also the in-plane hybridization between f electrons on neighboring sites.

Analogous to the relation between δ -Pu and PuGa_3 in the AuCu_3 crystal structure, α -Pu relates to PuGa_3 in the Ni_3Sn crystal structure. The crystal structures of both α -Pu and the low- T phase of PuGa_3 are the most stable and both have an AB stacking pattern. The α -Pu crystal structure stacks distorted close-packed Pu planes; replacing three of four Pu atoms with Ga removes the distortion to restore the symmetry in the close packed planes of PuGa_3 , which could relate to the stabilization of δ -Pu to low temperatures by adding a small amount of Ga.²⁴ The electronic specific heat coefficient γ differs dramatically between the low- T phase of PuGa_3 , where $\gamma = 220$ mJ/mol K², and α -Pu, where $\gamma = 17$ mJ/mol K² was measured.²⁵ Correspondingly, α -Pu can be well described by standard DFT methods,²⁶ while the work presented here shows that the low- T phase of PuGa_3 requires special attention be

paid to the strong $5f$ electron correlation, and allowing spin polarization does not suffice to describe the effects of the strong correlation.

ACKNOWLEDGMENTS

This research was supported by the Los Alamos National Laboratory, under the auspices of the National Nuclear Security Agency, by the U.S. Department of Energy under Grant No. LDRD-DR 20120024 (“Pu-242: A National Resource for the Fundamental Understanding of the $5f$ Electrons of Pu”). Many thanks go to in particular Eric Chisolm, Anders Niklasson, and John Wills as well as Eric Bauer, John Joyce, and Paul Tobash, for helpful and encouraging discussions. The author expresses a deep gratitude to Neil Henson for assistance with the ANDULU computational facility. Last, but not least, fond thanks go to Lucia Liên and Anna Lan for spurring alternative approaches to understanding.

-
- ¹ F. H. Ellinger, C. C. Land, and V. O. Struebing, J. Nucl. Mater. **12**, 226 (1964).
 - ² A. C. Larson, D. T. Cromer, and R. B. Roof, Jr, Acta Crystallographica **18**, 294 (1965).
 - ³ P. Boulet, E. Colineau, F. Wastin, P. Javorský, J. C. Griveau, J. Rebizant, G. R. Stewart, and E. D. Bauer, Phys. Rev. B **72**, 064438 (2005).
 - ⁴ P. Javorský, E. Colineau, F. Wastin, F. Jutier, J.-C. Griveau, P. Boulet, R. Jardin, and J. Rebizant, Phys. Rev. B **75**, 184501 (2007).
 - ⁵ I. Opahle, S. Elgazzar, K. Koepernik, and P. M. Oppeneer, Phys. Rev. B **70**, 104504 (2004).
 - ⁶ J. C. Lashley, A. Lawson, R. J. McQueeney, and G. H. Lander, Phys. Rev. B **72**, 054416 (2005).
 - ⁷ A. V. Postnikov and V. P. Antropov, Comp. Mat. Science **17**, 438 (2000).
 - ⁸ Y. Wang and Y. Sun, J. Phys.: Condens. Matter **12**, L311 (2000).
 - ⁹ P. Soderlind, Eur. Phys. Lett. **55**, 525 (2001).
 - ¹⁰ A. M. N. Niklasson, J. M. Wills, M. I. Katsnelson, I. A. Abrikosov, O. Eriksson, and B. Johansson, Phys. Rev. B **67**, 235105 (2003).
 - ¹¹ P. Soderlind, A. Landa, B. Sadigh, L. Vitos, and A. Ruban, Phys. Rev. B **70**, 144103 (2004).
 - ¹² A. Crocker, Journal of Nuclear Materials **41**, 167 (1971).
 - ¹³ G. Kresse and J. Furthmuller, Phys. Rev. B **54**, 11169 (1996).

- ¹⁴ G. Kresse and D. Joubert, Phys. Rev. B **59**, 1758 (1999).
- ¹⁵ J. P. Perdew, K. Burke, and M. Ernzerhof, Phys. Rev. Lett. **77**, 3865 (1996).
- ¹⁶ P. E. Blöchl, Phys. Rev. B **50**, 17953 (1994).
- ¹⁷ S. L. Dudarev, G. A. Botton, S. Y. Savrasov, C. J. Humphreys, and A. P. Sutton, Phys. Rev. B **57**, 1505 (1998).
- ¹⁸ D. Hobbs, G. Kresse, and J. Hafner, Phys. Rev. B **62**, 11556 (2000).
- ¹⁹ M. Marsman and J. Hafner, Phys. Rev. B **66**, 224409 (2002).
- ²⁰ L. Kleinman, Phys. Rev. B **21**, 2630 (1980).
- ²¹ A. H. MacDonald, W. E. Pickett, and D. D. Koelling, Journal of Physics C: Solid State Physics **13**, 2675 (1980).
- ²² J. Hubbard, Proceedings of the Royal Society of London. Series A, Mathematical and Physical Sciences **276**, 238 (1963).
- ²³ S. L. Dudarev, D. N. Manh, and A. P. Sutton, Philosophical Magazine Part B **75**, 613 (1997).
- ²⁴ O. J. Wick, *Plutonium Handbook, A Guide To The Technology* (Gordon and Breach, New York, 1967).
- ²⁵ J. C. Lashley, J. Singleton, A. Migliori, J. B. Betts, R. A. Fisher, J. L. Smith, and R. J. McQueeney, Phys. Rev. Lett. **91**, 205901 (2003).
- ²⁶ P. Soderlind, J. M. Wills, B. Johansson, and O. Eriksson, Phys. Rev. B **55**, 1997 (1997).